HHS Public Access

Author manuscript

Cell Rep. Author manuscript; available in PMC 2021 April 23.

Published in final edited form as:

Cell Rep. 2021 March 30; 34(13): 108925. doi:10.1016/j.celrep.2021.108925.

UPF1 reduces *C9orf72* HRE-induced neurotoxicity in the absence of nonsense-mediated decay dysfunction

Benjamin L. Zaepfel[1,2,8], **Zhe Zhang**[3,4,8], **Kirstin Maulding**[4,5], **Alyssa N. Coyne**[4,6], **Weiwei Cheng**[3,4], **Lindsey R. Hayes**[6], **Thomas E. Lloyd**[4,6,*], **Shuying Sun**[3,4,7,*], **Jeffrey D. Rothstein**[4,6,9,*]

[1]Biochemistry, Cellular and Molecular Biology Program, Johns Hopkins University School of Medicine, Baltimore, MD 21205, USA

[2]Molecular Biology and Genetics Department, Johns Hopkins University School of Medicine, Baltimore, MD 21205, USA

[3]Department of Pathology, Johns Hopkins University School of Medicine, Baltimore, MD 21205, USA

[4]Brain Science Institute, Johns Hopkins University School of Medicine, Baltimore, MD 21205, USA

[5]Cellular and Molecular Medicine Program, Johns Hopkins University School of Medicine, Baltimore, MD 21205, USA

[6]Department of Neurology, Johns Hopkins University School of Medicine, Baltimore, MD 21205, USA

[7]Department of Physiology, Johns Hopkins University School of Medicine, Baltimore, MD 21205, USA

[8]These authors contributed equally

[9]Lead contact

SUMMARY

Multiple cellular pathways have been suggested to be altered by the *C9orf72* GGGGCC (G_4C_2) hexanucleotide repeat expansion (HRE), including aspects of RNA regulation such as nonsense-mediated decay (NMD). Here, we investigate the role that overexpression of UPF1, a protein

*Correspondence: tlloyd4@jhmi.edu (T.E.L.), shuying.sun@jhmi.edu (S.S.), jrothstein@jhmi.edu (J.D.R.).

AUTHOR CONTRIBUTIONS

Conceived and designed the experiments, B.L.Z., Z.Z., K.M., T.E.L., S.S., and J.D.R.; performed the experiments, B.L.Z., Z.Z., K.M., A.N.C., W.C., and L.R.H.; analyzed the data, B.L.Z., Z.Z., and K.M.; contributed reagents and materials, B.L.Z., Z.Z., K.M., A.N.C., W.C., L.R.H., T.E.L., S.S., and J.D.R.; wrote the manuscript, B.L.Z., Z.Z., S.S., and J.D.R. with input from co-authors.

SUPPLEMENTAL INFORMATION

Supplemental information can be found online at https://doi.org/10.1016/j.celrep.2021.108925.

DECLARATION OF INTERESTS

The authors declare no competing interests.

INCLUSION AND DIVERSITY

One or more of the authors of this paper self-identifies as a member of the LGBTQ+ community.

involved in NMD, plays in mitigating neurotoxicity in multiple models of *C9orf72* ALS/FTD. First, we show that NMD is not altered in our endogenous induced pluripotent stem cell (iPSC)-derived spinal neuron (iPSN) model of *C9orf72* ALS (C9-ALS) or postmortem motor cortex tissue from C9-ALS patients. Unexpectedly, we find that UPF1 overexpression significantly reduces the severity of known neurodegenerative phenotypes without altering NMD function itself. UPF1 overexpression reduces poly(GP) abundance without altering the amount of repeat RNA, providing a potential mechanism by which UPF1 reduces dipeptide repeat (DPR) protein-mediated toxicity. Together, these findings indicate that UPF1 is neuroprotective in the context of C9-ALS, albeit independent of known UPF1-mediated NMD pathways.

Graphical abstract

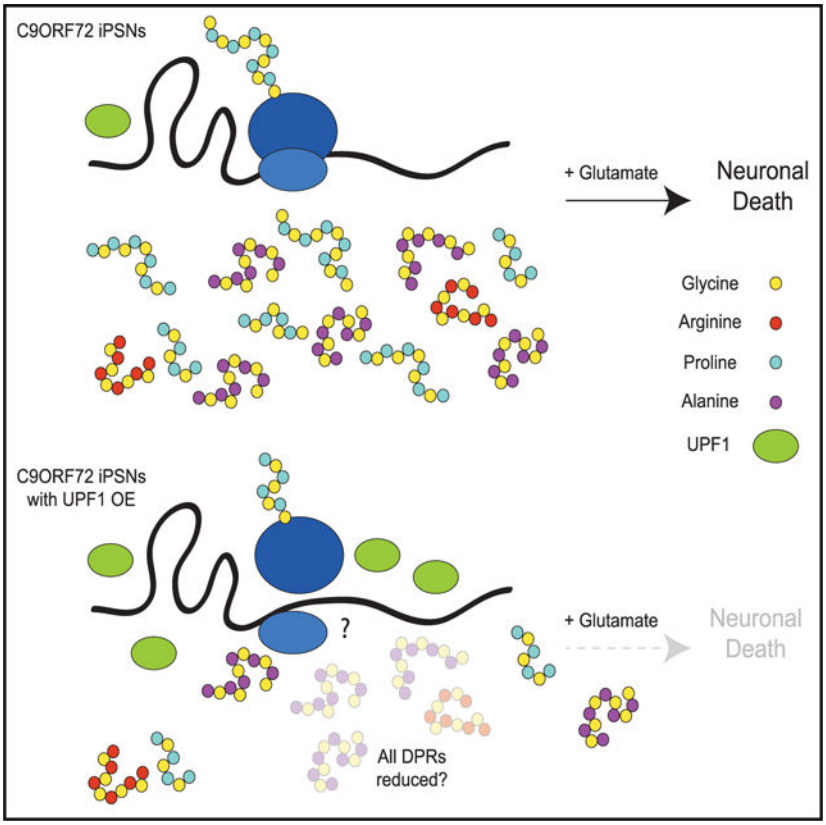

In brief

Zaepfel et al. show that UPF1 is neuroprotective in the context of C9-ALS. This neuroprotection is observed in multiple *in vitro* and *in vivo* models of C9-ALS. UPF1 mitigates toxicity independently of its role in nonsense-mediated decay but is dependent on its known RNA-binding and helicase activity.

INTRODUCTION

A G_4C_2 hexanucleotide repeat expansion (HRE) in the *C9orf72* gene is the most common known cause of familial and sporadic amyotrophic lateral sclerosis (ALS) and

frontotemporal dementia (FTD) (DeJesus-Hernandez et al., 2011; Renton et al., 2011). Pathologically, G_4C_2 (sense) and C_4G_2 (antisense) strand repeat RNA are produced via bi-directional transcription, and a portion of these transcripts is capable of accumulating into nuclear and cytoplasmic foci (Bajc Česnik et al., 2019; Lagier-Tourenne et al., 2013; Tran et al., 2015). A subset of repeat RNAs can be exported into the cytoplasm, where they undergo repeat-associated non-ATG (RAN) translation to produce a total of 5 dipeptide repeat (DPR) polypeptides: poly(GP), (GA), (GR), (PA), and (PR) (Ash et al., 2013; Mori et al., 2013; Zu et al., 2013). Finally, there is evidence to suggest that as a result of the HRE, impaired binding of RNA polymerase II at the promoter of the coding *C9orf72* gene may lead to decreased abundance of C9ORF72 protein (Boivin et al., 2020; Shi et al., 2018). However, the mechanisms by which these three pathological hallmarks of C9-ALS and C9-FTD lead to neurotoxicity in endogenous model systems remain largely unknown.

Dysfunction of multiple RNA metabolism pathways has been observed as a result of the HRE. Recently, three groups have published apparently discordant findings that nonsense-mediated decay (NMD) is either inhibited (Sun et al., 2020; Xu et al., 2019) or upregulated (Ortega et al., 2020) in different C9-ALS model systems.

NMD is an RNA surveillance pathway that identifies and degrades mRNA containing a premature termination codon (PTC), upstream open reading frames (uORFs), or long 3′ UTRs (Kebaara and Atkin, 2009; Kurosaki and Maquat, 2013, 2016; Maquat et al., 1981; Peccarelli and Kebaara, 2014). Recognition of each of these targets requires the phosphorylation of Up-frameshift 1 (UPF1) by the kinase serine/threonine protein kinase SMG1 (SMG1) (Isken et al., 2008). UPF1 is an RNA-binding protein that has helicase activity (Czaplinski et al., 1995) and can interact with other proteins involved in RNA surveillance pathways, like NMD (Isken et al., 2008; Maquat et al., 1981). Following phosphorylation by SMG1, UPF1 initiates NMD signal transduction, leading to the downstream degradation of the mRNA transcript and nascent peptide, as well as release and recycling of the 40S and 60S ribosomal subunits (Simms et al., 2017).

NMD is an important, translation-dependent process to prevent the accumulation of truncated peptides that may adopt dominant-negative or other deleterious functions. The most recent, and perhaps most direct, investigation of NMD function in a C9-ALS model identifies that the apparent decrease in NMD function in the context of high poly(PR) concentrations is entirely accounted for by a reduction in translation, not a direct inhibition of NMD (Sun et al., 2020).

To thoroughly and directly assess NMD function in the context of C9-ALS, we identified a panel of NMD mRNA substrates using a potent and specific NMD inhibitor, SMG1i. SMG1i inhibits phosphorylation of UPF1 by SMG1, thereby preventing the downstream degradation of NMD substrates. Using this mRNA panel, we provide evidence that neither the steady-state abundance nor the stability of NMD substrates is altered in multiple different patient induced pluripotent stem cell (iPSC)-derived neuronal cell lines containing the endogenous HRE that best mimics real human disease (Coyne et al., 2020; Donnelly et al., 2013; Zhang et al., 2015). Interestingly, we find UPF1 overexpression (OE) rescues multiple phenotypes associated with HRE-induced degeneration in multiple models of C9 ALS, despite the

absence of an underlying NMD defect. This rescue may, in part, occur by reducing the abundance of DPRs, but not repeat RNA. Our data, paired with previous findings that UPF1 is neuroprotective in C9 ALS, highlight UPF1, but not NMD, as a potential therapeutic target in neurodegeneration.

RESULTS

NMD substrate abundance and stability are not altered in C9 iPSNs or postmortem motor cortex

To assess whether NMD was functionally altered by the *C9orf72* HRE, we first validated the identity of endogenous neuronal NMD substrates, since this pathway has been shown to have cell-type-specific efficiency (Linde et al., 2007). By treating cells with 500 nM SMG1i, a small-molecule inhibitor of NMD, we significantly reduced SMG1-dependent phosphorylation of UPF1 (Figures S1A–S1D). Both HEK293T cells and iPSC-derived spinal neurons (iPSNs) exhibit substantial increases in the abundance of previously identified NMD substrates (UPF1, SMG5, SMG7, GADD45A, and ATF4) (Colombo et al., 2017) following 24 h treatment with SMG1i (Figures S1E and S1F). Importantly, the abundance of beta-actin mRNA, a negative control substrate, is unaffected by SMG1i treatment (Figures S1E and S1F).

Using this panel of five endogenous neuronal NMD substrates, we sought to determine if their baseline levels were altered in C9-ALS iPSNs or patient brain tissue. qRT-PCR analysis demonstrates no change in the steady-state abundance of any of these five substrates in C9-ALS iPSNs (Figure 1A) and postmortem motor cortex (Figure 1B) relative to controls. To further assess NMD function at the RNA level, we used actinomycin D, a potent inhibitor of transcription, to determine whether the stability of these NMD substrates is altered in C9-ALS iPSNs. Over 5 h, we measured the abundance of NMD substrates relative to XPNPEP1 mRNA and observed no significant differences between control and C9-ALS iPSNs within the subset of patient lines evaluated (Figure 1C). To account for potential differences in the loading controls themselves, we compared NMD substrate abundance to three different housekeeping genes (XPNPEP1 in Figure 1 and GAPDH and beta-actin in Figure S2), which all yielded consistent results.

Together, our data suggest that contrary to previous findings from DPR OE models of *C9orf72* ALS (Ortega et al., 2020; Xu et al., 2019), we observe no defect in NMD at the level of RNA substrates in an endogenous human C9 iPSN model as well as ALS postmortem motor cortex. These results demonstrate that NMD function is not globally defective in human C9-ALS.

UPF1 expression is unaltered in C9 iPSNs and patient postmortem motor cortex

Consistent with the lack of functional changes in UPF1 NMD activity in C9 iPSNs, we observed no change in the total protein abundance of UPF1 in C9 iPSNs via western blot or postmortem motor cortex via immunofluorescence, compared to controls (Figures S3A–S3D). Importantly, we also observed no change in the level of UPF1 phosphorylation in C9 iPSNs (Figures S3A and S3B), which is required for NMD-dependent mRNA degradation

(Isken et al., 2008). Altogether, this suggests that the endogenous HRE does not significantly alter UPF1 abundance or phosphorylation in patient cultured neurons or brain tissue, supporting the notion that NMD is unaltered in C9-ALS.

UPF1 OE mitigates neurodegenerative phenotypes in multiple models of *C9orf72* ALS

Recent studies have demonstrated that UPF1 expression can modulate DPR- or HRE-induced degenerative phenotypes in various OE models of C9-ALS (Ortega et al., 2020; Sun et al., 2020; Xu et al., 2019). To validate this, we utilized a *Drosophila melanogaster* model of *C9orf72* ALS that expresses 30 G_4C_2 repeats (30R) upstream of a polyadenylation signal (Xu et al., 2013). We observe that expression of this repeat specifically in photoreceptors using a GMR-Gal4 driver leads to progressive age-dependent eye degeneration (Figures 2A and 2B), consistent with our previous study showing a marked loss of photoreceptors (Zhang et al., 2015). The degeneration caused by 30R expression in the eye is significantly suppressed by co-expression of UPF1, while it is enhanced by UPF1 knockdown via RNAi (Figures 2A and 2B).

Hyperexcitability of neurons is a long-standing observation in patients with ALS (Vucic and Kiernan, 2006; Vucic et al., 2008). We have previously established that C9-ALS iPSNs are sensitive to exogenous glutamate stress (Donnelly et al., 2013) and that assays of glutamate sensitivity serve as a general readout of cellular stress and a paradigm to identify pathways to mitigate this stress. Using this readout of cellular death, by assaying propidium iodide incorporation, we find that 10 μM glutamate treatment leads to significant death of C9-ALS, but not control iPSNs (Figures 2C and 2D). Importantly, C9-ALS iPSNs OE UPF1 exhibited significantly reduced death compared to those OE GFP (Figures 2C and 2D). Taken together, these findings demonstrate that UPF1 OE mitigates *C9orf72* HRE-mediated neurodegenerative phenotypes *in vivo* and *in vitro*.

UPF1 OE does not alter NMD efficiency

Despite the lack of functional defects of UPF1 in C9-ALS iPSNs, UPF1 OE can reduce the HRE-induced toxicity (Figure 2). We tested whether UPF1 OE may increase NMD efficiency and reduce the abundance of potentially toxic transcripts. However, qRT-PCR analysis indicates that UPF1 OE in HEK293T cells or iPSNs does not lead to any change in the abundance of endogenous NMD substrates (Figures S3E and S3F). This agrees with previous reports of UPF1 function, suggesting that increasing the abundance of UPF1 does not significantly increase the recognition and degradation of endogenous NMD substrates (Dehecq et al., 2018). This indicates that the rescue effect of UPF1 OE is not mediated through the regulation of NMD function.

C9orf72 sense-strand repeat RNA is unlikely to be a direct NMD substrate

Since UPF1 OE is mitigating HRE-induced toxicity independently of NMD, we sought to determine whether UPF1 regulates the abundance of DPRs or repeat RNA, which are the primary sources of C9 HRE toxicity. We hypothesized that if the repeat RNA is an NMD substrate, OE of UPF1 may function to reduce its toxicity by targeting it for degradation via NMD. To test this, we treated C9-ALS iPSNs with SMG1i and performed qRT-PCR to quantify the abundance of the repeat RNA. We observed no change in the repeat RNA

abundance after 24 h (Figure 3A), at a time when all the validated NMD substrates demonstrate significantly increased abundance (Figure S1F). Interestingly, the repeat RNA shows modest increase in abundance with prolonged exposure to SMG1i (Figure 3A), which may be an indirect effect of alterations in some unknown pathway whose function is regulated downstream of NMD.

An additional indication that the repeat RNA is an NMD substrate would be strong binding by UPF1. To assess this potential interaction, we performed immunoprecipitation (IP) of UPF1 from C9-ALS iPSNs (Figure 3B) and analyzed the IP fraction for enrichment of the repeat RNA. While ATF4, a validated NMD substrate, was strongly enriched (~9-fold enriched, $p = 0.0132$) in the IP fraction, the sense-strand repeat RNA only showed modest enrichment (~2.9-fold enriched, $p = 0.7159$) when compared to GAPDH, which is not an NMD substrate (Figure 3C). Therefore, while UPF1 demonstrates minor affinity for the sense-strand repeat RNA, it is unlikely that UPF1 targets it for degradation via NMD.

UPF1 OE reduces poly-GP in C9 iPSNs

We next used previously established dual-luciferase splicing reporters to test for DPR production from the intronic HRE (Cheng et al., 2019). In this system, the Nanoluc luciferase (Nluc) is produced through RAN translation of GGGGCC repeats located in the first intron of *C9ORF72*, and the Firefly luc (Fluc) is fused with the AUG start codon in exon2 (Cheng et al., 2019). Small interfering RNA (siRNA) knockdown of UPF1 led to a significant increase in abundance of all three sense DPR reading frames (Figures 4A and S4A–S4C), while UPF1 OE decreased DPR levels in the reporters (Figure S4D). The UPF1-dependent decrease in DPR levels in the HeLa reporters requires its RNA-binding and helicase function, as OE of mutant UPF1 (R843C, which lacks these functions) had no effect on DPR levels (Figure S4D).

As reducing UPF1 can elevate DPR reporter levels in artificial OE model systems, we next tested whether UPF1 OE in C9 iPSNs would reduce endogenous poly(GP) abundance. UPF1 OE in C9 iPSNs indeed led to a significant decrease of endogenous poly(GP) (Figure 4B), as detected with a previously reported ELISA-based assay (Cheng et al., 2019). Notably, this reduction of poly(GP) in C9 iPSNs occurred without alterations in the abundance of the sense-strand repeat RNA in C9-ALS iPSNs (Figure 4C). siRNA knockdown of UPF1 led to an increase in poly(GP) levels in C9-ALS iPSNs without altering the abundance of sense-strand repeat or *C9orf72* coding RNA (Figures S4E and S4F). Paired with the observation that UPF1 OE does not alter NMD function, these findings demonstrate a strong relationship between UPF1 and DPR abundance and suggest that there are NMD-independent pathways by which UPF1 can modulate DPR levels.

DISCUSSION

The connection between ALS and UPF1 has become increasingly apparent in recent years. Multiple groups have assessed the role that UPF1 plays in neuronal degeneration caused by ALS-linked mutations. UPF1 OE was shown to improve survival of primary mouse neurons that OE TDP-43 (wild type [WT] and A315T), and this rescue required the RNA-binding and helicase functions of UPF1 (Barmada et al., 2015). Another group describes a

hyperactive-UPF1 model in which cells expressing ALS-linked FUS variants exhibit increased (and toxic) NMD activity due to loss of UPF1 autoregulation (Kamelgarn et al., 2018). Finally, three recent publications report that UPF1 OE is neuroprotective in distinct models of *C9orf72* ALS (Ortega et al., 2020; Sun et al., 2020; Xu et al., 2019).

Despite their concordance on the neuroprotective role that UPF1 plays in these *C9orf72* ALS models, these three groups provide disparate interpretations of whether UPF1 is hypo- or hyper-activated by the *C9orf72* HRE. Xu et al. (2019) propose that NMD is inhibited upon OE of arginine-rich DPRs. However, given that NMD is a translation-dependent process and OE arginine-rich DPRs significantly reduce translation (Moens et al., 2019), the authors did not rule out the possibility that NMD substrates are stabilized in their model entirely due to this reduced translation. Indeed, Sun et al. (2020) rigorously demonstrate that the apparent NMD defect that arises from high concentrations of arginine-rich DPRs is a direct result of reduced translation, not alteration of the NMD pathway itself. On the other hand, Ortega et al. (2020) suggest that NMD is upregulated in C9 iPSNs based on increased abundance of SMG1 and phosphorylated UPF1, although they provide no evidence for altered NMD substrate stability. This disagreement regarding the functionality of NMD in neurons harboring the *C9orf72* HRE warranted a closer look at NMD function at the level of RNA. Through the evaluation of a panel of NMD RNA substrates, we found that NMD function is unaltered in neurons harboring the endogenous *C9orf72* HRE and is unlikely to be directly implicated in C9 ALS pathogenesis (Figure 1).

However, in agreement with the findings presented by previous groups (Ortega et al., 2020; Sun et al., 2020; Xu et al., 2019), we observe that UPF1 OE mitigates *C9orf72* HRE-induced neurodegenerative phenotypes in multiple OE and endogenous models including *Drosophila* photoreceptor degeneration (Figures 2A and 2B) and C9 iPSNs (Figures 2C and 2D). We hypothesized that UPF1 OE may be reducing the observed degeneration by upregulating NMD, in turn reducing the abundance of some toxic contributor(s). Yet, UPF1 OE does not, in the absence of an underlying NMD defect, alter the abundance of known endogenous NMD substrates in HEK293T cells or iPSNs (Figures S3E and S3F), which agrees with previous findings (Dehecq et al., 2018). Thus, UPF1 OE does not globally increase the efficiency of NMD substrate degradation. This does not exclude the possibility that UPF1 OE is specifically affecting the abundance of an untested substrate or substrates.

Since UPF1 OE does not alter the abundance of the endogenous NMD substrates evaluated, it may prevent toxicity by reducing the abundance of DPRs or the HRE repeat RNA. Indeed, C9 iPSNs OE UPF1 exhibit significantly decreased poly(GP) abundance compared to C9 iPSNs OE GFP (Figure 4B). In contrast, UPF1 OE had no effect on the abundance of the sense-strand repeat RNA (Figure 4C). Although we have not tested whether UPF1 OE alters the abundance of the other four DPRs in iPSNs, we hypothesize that this UPF1-mediated rescue may occur by reducing RAN translation of the sense-strand repeat RNA without affecting its metabolism, as has been observed with another helicase, DDX3X (Cheng et al., 2019). While we do not currently have assays to accurately quantify the effect of UPF1 alterations on poly(GA) and poly(GR) abundance, we provide evidence using a powerful HeLa reporter toolset that UPF1 OE reduces abundance of all the sense-strand DPRs, while UPF1 knockdown increases their abundance (Figures 4 and S4).

Although the best-known functions of UPF1 involve degradation of PTC-containing mRNAs, it is possible that its neuroprotective properties derive from some other function. As a general RNA-binding protein, we still do not fully understand how (or if) UPF1 exhibits selectivity to bind mRNAs that are not slated for degradation. Here, we demonstrate that the DPR-reducing effect of UPF1 OE is mediated through its RNA-binding and helicase function (Figure S4). Paired with the absence of NMD alterations when we OE UPF1, this substantiates the importance of non-NMD function of UPF1 as an RNA-binding protein.

In addition to our findings that UPF1 acts as a strong modulator of neurodegeneration *in vivo* and *in vitro*, we determine that the sense-strand repeat RNA is unlikely to be an NMD substrate, contrary to a prior report (Ortega et al., 2020). We do not see strong stabilization of the sense-strand repeat RNA upon treatment with SMG1i, nor do we see strong binding of this RNA by UPF1 (Figure 3). These two observations support that the repeat RNA is not targeted for degradation by the NMD pathway. This is perhaps unsurprising, as a previous report demonstrates that specific inhibition of RAN translation via RPS25 knockdown does not alter the abundance of the sense-strand repeat RNA (Yamada et al., 2019). If the repeat RNA were, in fact, an NMD substrate, one would expect its abundance to *increase* following reduction of translation.

Clearly, there exists controversy over whether and how NMD is altered in the context of C9 ALS, and our work suggests this is not an altered pathway in patient-derived post-mortem tissue or iPSNs. Yet, our work, along with others', concludes that UPF1 OE is neuroprotective. While the DPR-reducing function of UPF1 is independent of its role in NMD, the precise mechanistic explanation for the DPR reduction remains the topic of future investigations. Collectively, these studies support the notion that increasing the abundance of UPF1 is a valid therapeutic strategy.

STAR★METHODS

RESOURCE AVAILABILITY

Lead contact—Further information and requests for resources and reagents should be directed to and will be fulfilled by Jeffrey D. Rothstein (lead contact, jrothstein@jhmi.edu).

Materials availability—The plasmids generated for this manuscript are available upon requests directed to Jeffrey D. Rothstein (lead contact, jrothstein@jhmi.edu).

Data and code availability—This study did not generate or analyze datasets or code.

EXPERIMENTAL MODEL AND SUBJECT DETAILS

HeLa, HEK293T, and iPSC neuron differentiation—HeLa Flp-In dual luciferase reporter cells and HEK293T cells were cultured in DMEM supplemented with 10% (v/v) FBS and 100 U/ml penicillin and 100 μg/ml streptomycin. iPSCs were maintained and differentiated as previously described (Coyne et al., 2020).

METHOD DETAILS

Plasmids—Lentiviral vectors expressing UPF1 was engineered by replacing DDX3X from Lenti-DDX3X-FLAG vector (Cheng et al., 2019) with UPF1 by XbaI and BamHI sites (UPF1Forward; UPF1 Reverse).

The Lenti-UPF1 (R843C)-FLAG plasmid was generated from the Lenti-UPF1-FLAG plasmid using Gibson Assembly (New England Biolabs E5510S). First, two PCR fragments were generated using four different primers complementary to Lenti-UPF1-FLAG. Fragment 1 was generated via PCR using R843C Fragment 1 Forward and R843C Fragment 1 Reverse. Fragment 2 was generated using R843C Fragment 2 Forward and R843C Fragment 2 Reverse. The overlaps between these two fragments allowed for plasmid generation via Gibson Assembly®, using the manufacturer-provided protocol. R843C mutation was validated by Sanger Sequencing using R843 Sequencing primer.

Cell transfection—Lipofectamine RNAiMAX (Invitrogen) was used to transfect siRNAs into HeLaFlp-In dual luciferase reporter cells. ON-TARGETplus human UPF1 pooled siRNAs or Silencer select UPF1 siRNA (s11926) and ON-TARGETplus Non-Targeting siRNA (GE Dharmacon) were transfected at 25nM 16 hours after the cells were seeded in 24-well plate. The reporter gene expression was induced by 2 μg/ml tetracycline at 48 h after transfection, and samples were collected after another 48 h. TransIT®-LT1 Transfection Reagent (Mirus) was used to transfect pcDNA3.1-Flag-UPF1. Cells were seeded 24 hours after transfection and induced by 2 μg/ml tetracycline for another 48h. Cells were lysis with 5X passive lysis buffer. Fluc and Nluc luciferase activities were measured by Nano-Glo Dual Luciferase Assay (Promega) on Tecan Infinite 200 PRO. NLuc levels were normalized to total protein or FLuc. Protein concentration was quantified by BCA Assay (ThermoFisher Scientific).

24 hours after splitting, HEK293T cells were transfected using Lipofectamine 3000 (Thermo Fisher Scientific). Experiments were performed 24 hours post-transfection. Expression of GFP and exogenous UPF1 was validated by qRT-PCR and Western Blot.

On day 13 of differentiation, iPSNs were transfected with 100nM siRNA by Lipofectamine RNAiMAX or transduced with lentivirus and then assayed at 30–32 days post-differentiation.

Drosophila* husbandry and eye degeneration analysis—Drosophila* were raised on standard cornmeal-molasses food at 25° C. For eye degeneration, GMR-Gal4, UAS-30R/CyO, twi-Gal4, UAS-GFP were crossed to UAS modifier lines or background controls. Flies expressing GMR-Gal4 and UAS-30R or UAS-30R and a modifier were selected and aged at 25° C for 15 days. Eye degeneration was quantified as previously described (Ritson et al., 2010).Degeneration was quantified out of a total of 20 points. Points were added for complete loss of interommatidial bristles, necrotic patches, retinal collapse, loss of ommatidial structure, or loss of eye pigmentation. Eye images were obtained using a Nikon SMZ 1500 Microscope and Infinity 3 Luminera Camera with Image Pro Insight 9.1 software.

Analysis of eye degeneration was carried out in Prism version 8

Glutamate-induced neurotoxicity Assay: To test the glutamate-induced excitotoxicity, control and *C9orf72*-ALS iPSNs with either GFP-FLAG or UPF1-FLAG overexpression (18 days after infection) were treated with 10 μM L-glutamate for 4hrs. Then the cells were stained with Hoechst33342 (5 μg/ml) and Propidium Iodide (1 μg/ml) for 30 min to visualize total and dead cells. Cells were washed thoroughly with PBS, followed by immunofluorescence of FLAG tag to confirm the infection efficiency.

qRT-PCR—Samples were briefly rinsed in 1x DPBS with calcium and magnesium, then lysed in 6 well plates using TriZol (Thermo Fisher Scientific). Total RNA was isolated using the standard TriZol protocol. The concentration of RNA samples was determined using a NanoDrop 1000 spectrophotometer (Thermo Fisher Scientific). 2 ug RNA was used for cDNA synthesis using the High Capacity cDNA Reverse Transcription Kit (Thermo Fisher Scientific). qRT-PCR reactions were performed using TaqMan Fast Advanced Master Mix and an Applied biosystems StepOnePlus Real Time PCR machine (Applied Biosystems) using previously described (Lagier-Tourenne et al., 2013) or commercially available primer-probe sets (Thermo Fisher Scientific). mRNA abundance was measured relative to *XPNPEP1, GAPDH, or ACTB* mRNA.

Technical duplicates or triplicates were utilized within each qRT-PCR plate. A negative control (NTC) was used for each probe on each qRT-PCR plate to ensure the absence of detected background signal. All direct pairwise comparisons are made within qRT-PCR plates (no direct comparisons were made between different plates) to account for potential plate-to-plate variation. Delta CT values are plotted to demonstrate inherent variation within control and experimental samples, as well as to represent the relative abundance of the mRNAs of interest when compared to reference mRNA.

Meso scale discovery (MSD) ELISA—Poly(GP) ELISA assays were performed as previously described (Cheng et al., 2019).

Western blots—Samples were harvested in 1x PBS, then spun down in a microcentrifuge and the PBS was aspirated. Samples were resuspended in RIPA buffer (Millipore Sigma) containing 1x protease inhibitor cocktail (Millipore Sigma). Human tissue was homogenized in the same RIPA buffer noted above. Samples were spun at 12,000 g for 15 minutes to remove debris, and the supernatant was transferred to a new tube. Protein concentrations were determined using the DC Protein Assay Kit (Bio-Rad). 6x Laemmli buffer (12% SDS, 50% glycerol, 3% TrisHCl pH 7.0, 10% 2-mercaptoethanol in dH2O, bromophenol blue to color) was added to a final 1x concentration. 10uq protein was loaded into 4%–20% acrylamide gels and run until the dye front reached the bottom. Protein was transferred onto nitrocellulose membrane (Bio-Rad). Following transfer, blots were blocked for 1 hour in 5% milk in 1x TBS-Triton (0.1%). Blots were probed overnight (approximately 16 hours) at 4 degrees. Blots were washed four times in 1x TBST for 10 minutes each, probed with secondary antibody for 1 hour at room temperature, and washed another four times in 1x TBST for 10 minutes each. ECL substrate (Millipore Sigma, Thermo Fisher Scientific) was applied for 30 s, then images were taken using the GE Healthcare ImageQuant LAS 4000.

Images were quantified using FIJI. Protein abundance was normalized to total protein levels using the BLOT-FastStain Kit (G-Biosciences).

Immunofluorescence staining and imaging—HEK293T cells were fixed and stained as previously described (Coyne et al., 2020) using Rabbit anti-phospho-UPF1 antibody (Millipore Sigma) at a 1:250 dilution and AlexaFluor 488 conjugated Goat anti-Rabbit secondary antibody (Thermo Fisher Scientific) at a 1:1000 dilution in a 24-well glass-bottom plate (Cellvis). 9 sites in each well were imaged using a 20x objective on an ImageExpress Micro Confocal High-Content Imaging System (Molecular Devices).

iPSNs were fixed with 4% (v/v) para-formaldehyde in PBS for 10 min, permeabilized in 0.2% (v/v) Triton X-100 for 10 min, blocked in 1% bovine serum albumin and 2% goat serum for 1h, incubated with primary antibodies overnight at 4°C, washed with PBS, and finally incubated with Alexa Fluor 488/647 conjugated secondary antibodies (ThermoFisher Scientific). Cells were imaged with a Zeiss 800 Airyscan microscope.

Human tissue immunofluorescence—Human tissue was stained and imaged using a Zeiss Axioimager Z2 fluorescent microscope equipped with an apotome2 module as previously reported (Coyne et al., 2020). UPF1 intensity (Atlas Antibodies HPA020857) was quantified using FIJI.

Immunoprecipitation—Per sample, 50 uL Protein G Dynabeads (Invitrogen) were briefly rinsed in 1x PBS, then incubated with 10 ug of rabbit anti-UPF1 antibody (Abcam ab109363) diluted in 200uL of 1x PBS containing 0.02% Tween-20 at room temperature for 10 minutes on a rotator. Samples were lysed in 1mL IP Lysis buffer (Thermo Fisher Scientific 87787) containing 1x EDTA-free protease inhibitor cocktail (Roche) and 400u/mL RNase inhibitor (Thermo Fisher Scientific 10777019) by vortexing for 45 s. Samples were centrifuged at ~600 g for 10 minutes at 4 degrees to remove debris, and supernatant was transferred to a new tube. 50uL of sample were taken as input for protein and RNA isolation (added 6x Laemmli to 1x concentration for protein samples), and the remaining sample was incubated with antibody-bound beads for 2 hours on a rotator at 4 degrees. Samples were placed on a magnet and the supernatant removed. 200uL of the IP lysis buffer mix noted above was added to the samples and rotated at 4 degrees for 10 minutes, repeated for a total of 3 washes. Samples were resuspended in 50uL of IP lysis buffer, and 10uL of this volume was taken for protein analysis (added 6x Laemmli to 1x concentration), with the other 40uL used for RNA isolation.

Transcription inhibition assay—On D32 post-differentiation, iPSNs were treated with Stage 3 media (Coyne et al., 2020) containing 10ug/mL actinomycin D. Samples were harvested at the time points indicated and total RNA was isolated for qRT-PCR analysis.

SMG1i treatment—For assays involving SMG1i, cells were treated with the appropriate media containing 0.1% DMSO or 500nM SMG1i for 24 hours.

QUANTIFICATION AND STATISTICAL ANALYSIS

Quantification methods, statistical analyses, and sample sizes for each experiment are detailed in their respective figure legends. For iPSN experiments where certain lines were assayed multiple times, shapes are used to indicate replicated data points from each line. Statistical significance from those data are calculated from the mean of the replicates for each line.

Supplementary Material

Refer to Web version on PubMed Central for supplementary material.

ACKNOWLEDGMENTS

We thank the ALS patients and their families for essential contributions to this research and the Target ALS Human Postmortem Tissue Core for providing postmortem human tissue. We thank Xiaopei Tang and Weibo Zhou for expert assistance with iPSC differentiations and Lin Xue and Lindsey Hayes for assistance with ELISAs. We also thank members of the Green lab, including Dr. Rachel Green and Dr. Boris Zinshteyn, for their expertise in RNA biology. The SMG1i compound was generously provided by the Cystic Fibrosis Foundation. This work was supported by T32GM007445 (for B.L.Z.) and funding from the Robert Packard Center for ALS Research and NIH-NINDS (R01NS094239 to T.E.L. and J.D.R., R01NS107347 to S.S., K08NS104273 to L.R.H.), Target ALS (S.S.), and ALSA (S.S. and T.E.L.). Z.Z. and A.N.C. are recipients of the ALSA Milton Safenowitz Postdoctoral Fellowship.

REFERENCES

Ash PE, Bieniek KF, Gendron TF, Caulfield T, Lin WL, Dejesus-Hernandez M, van Blitterswijk MM, Jansen-West K, Paul JW 3rd, Rademakers R, et al. (2013). Unconventional translation of C9ORF72 GGGGCC expansion generates insoluble polypeptides specific to c9FTD/ALS. Neuron 77, 639–646. [PubMed: 23415312]

Bajc Česnik A, Darovic S, Prpar Mihevc S, Štalekar M, Malnar M, Mo-taln H, Lee YB, Mazej J, Pohleven J, Grosch M, et al. (2019). Nuclear RNA foci from *C9ORF72* expansion mutation form paraspeckle-like bodies. J. Cell Sci 132, jcs224303. [PubMed: 30745340]

Barmada SJ, Ju S, Arjun A, Batarse A, Archbold HC, Peisach D, Li X, Zhang Y, Tank EM, Qiu H, et al. (2015). Amelioration of toxicity in neuronal models of amyotrophic lateral sclerosis by hUPF1. Proc. Natl. Acad. Sci. USA 112, 7821–7826. [PubMed: 26056265]

Boivin M, Pfister V, Gaucherot A, Ruffenach F, Negroni L, Sellier C, and Charlet-Berguerand N (2020). Reduced autophagy upon C9ORF72 loss synergizes with dipeptide repeat protein toxicity in G4C2 repeat expansion disorders. EMBO J. 39, e100574. [PubMed: 31930538]

Cheng W, Wang S, Zhang Z, Morgens DW, Hayes LR, Lee S, Portz B, Xie Y, Nguyen BV, Haney MS, et al. (2019). CRISPR-Cas9 Screens Identify the RNA Helicase DDX3X as a Repressor of C9ORF72 (GGGGCC)n Repeat-Associated Non-AUG Translation. Neuron 104, 885–898.e8. [PubMed: 31587919]

Colombo M, Karousis ED, Bourquin J, Bruggmann R, and Muhlemann O (2017). Transcriptome-wide identification of NMD-targeted human mRNAs reveals extensive redundancy between SMG6- and SMG7-mediated degradation pathways. RNA 23, 189–201. [PubMed: 27864472]

Coyne AN, Zaepfel BL, Hayes L, Fitchman B, Salzberg Y, Luo EC, Bowen K, Trost H, Aigner S, Rigo F, et al. (2020). G_4C_2 Repeat RNA Initiates a POM121-Mediated Reduction in Specific Nucleoporins in C9orf72 ALS/FTD. Neuron 107, 1124–1140.e11. [PubMed: 32673563]

Czaplinski K, Weng Y, Hagan KW, and Peltz SW (1995). Purification and characterization of the Upf1 protein: a factor involved in translation and mRNA degradation. RNA 1, 610–623. [PubMed: 7489520]

Dehecq M, Decourty L, Namane A, Proux C, Kanaan J, Le Hir H, Jacquier A, and Saveanu C (2018). Nonsense-mediated mRNA decay involves two distinct Upf1-bound complexes. EMBO J. 37, e99278. [PubMed: 30275269]

DeJesus-Hernandez M, Mackenzie IR, Boeve BF, Boxer AL, Baker M, Rutherford NJ, Nicholson AM, Finch NA, Flynn H, Adamson J, et al. (2011). Expanded GGGGCC hexanucleotide repeat in noncoding region of C9ORF72 causes chromosome 9p-linked FTD and ALS. Neuron 72, 245–256. [PubMed: 21944778]

Donnelly CJ, Zhang PW, Pham JT, Haeusler AR, Mistry NA, Vidensky S, Daley EL, Poth EM, Hoover B, Fines DM, et al. (2013). RNA toxicity from the ALS/FTD C9ORF72 expansion is mitigated by antisense intervention. Neuron 80, 415–428. [PubMed: 24139042]

Isken O, Kim YK, Hosoda N, Mayeur GL, Hershey JW, and Maquat LE (2008). Upf1 phosphorylation triggers translational repression during nonsense-mediated mRNA decay. Cell 133, 314–327. [PubMed: 18423202]

Kamelgarn M, Chen J, Kuang L, Jin H, Kasarskis EJ, and Zhu H (2018). ALS mutations of FUS suppress protein translation and disrupt the regulation of nonsense-mediated decay. Proc. Natl. Acad. Sci. USA 115, E11904–E11913. [PubMed: 30455313]

Kebaara BW, and Atkin AL (2009). Long 3′-UTRs target wild-type mRNAs for nonsense-mediated mRNA decay in Saccharomyces cerevisiae. Nucleic Acids Res. 37, 2771–2778. [PubMed: 19270062]

Kurosaki T, and Maquat LE (2013). Rules that govern UPF1 binding to mRNA 3′ UTRs. Proc. Natl. Acad. Sci. USA 110, 3357–3362. [PubMed: 23404710]

Kurosaki T, and Maquat LE (2016). Nonsense-mediated mRNA decay in humans at a glance. J. Cell Sci 129, 461–467. [PubMed: 26787741]

Lagier-Tourenne C, Baughn M, Rigo F, Sun S, Liu P, Li HR, Jiang J, Watt AT, Chun S, Katz M, et al. (2013). Targeted degradation of sense and antisense C9orf72 RNA foci as therapy for ALS and frontotemporal degeneration. Proc. Natl. Acad. Sci. USA 110, E4530–E4539. [PubMed: 24170860]

Linde L, Boelz S, Neu-Yilik G, Kulozik AE, and Kerem B (2007). The efficiency of nonsense-mediated mRNA decay is an inherent character and varies among different cells. Eur. J. Hum. Genet 15, 1156–1162. [PubMed: 17625509]

Maquat LE, Kinniburgh AJ, Rachmilewitz EA, and Ross J (1981). Unstable beta-globin mRNA in mRNA-deficient beta o thalassemia. Cell 27, 543–553. [PubMed: 6101206]

Moens TG, Niccoli T, Wilson KM, Atilano ML, Birsa N, Gittings LM, Holbling BV, Dyson MC, Thoeng A, Neeves J, et al. (2019). C9orf72 arginine-rich dipeptide proteins interact with ribosomal proteins in vivo to induce a toxic translational arrest that is rescued by eIF1A. Acta Neuropathol. 137, 487–500. [PubMed: 30604225]

Mori K, Weng SM, Arzberger T, May S, Rentzsch K, Kremmer E, Schmid B, Kretzschmar HA, Cruts M, Van Broeckhoven C, et al. (2013). The C9orf72 GGGGCC repeat is translated into aggregating dipeptide-repeat proteins in FTLD/ALS. Science 339, 1335–1338. [PubMed: 23393093]

Ortega JA, Daley EL, Kour S, Samani M, Tellez L, Smith HS, Hall EA, Esengul YT, Tsai YH, Gendron TF, et al. (2020). Nucleocytoplasmic Proteomic Analysis Uncovers eRF1 and Nonsense-Mediated Decay as Modifiers of ALS/FTD C9orf72 Toxicity. Neuron 106, 90–107.e13. [PubMed: 32059759]

Peccarelli M, and Kebaara BW (2014). Regulation of natural mRNAs by the nonsense-mediated mRNA decay pathway. Eukaryot. Cell 13, 1126–1135. [PubMed: 25038084]

Renton AE, Majounie E, Waite A, Simón-Sánchez J, Rollinson S, Gibbs JR, Schymick JC, Laaksovirta H, van Swieten JC, Myllykangas L, et al.; ITALSGEN Consortium (2011). A hexanucleotide repeat expansion in C9ORF72 is the cause of chromosome 9p21-linked ALS-FTD. Neuron 72, 257–268. [PubMed: 21944779]

Ritson GP, Custer SK, Freibaum BD, Guinto JB, Geffel D, Moore J, Tang W, Winton MJ, Neumann M, Trojanowski JQ, et al. (2010). TDP-43 mediates degeneration in a novel Drosophila model of disease caused by mutations in VCP/p97. J. Neurosci 30, 7729–7739. [PubMed: 20519548]

Shi Y, Lin S, Staats KA, Li Y, Chang WH, Hung ST, Hendricks E, Linares GR, Wang Y, Son EY, et al. (2018). Haploinsufficiency leads to neurodegeneration in C9ORF72 ALS/FTD human induced motor neurons. Nat. Med 24, 313–325. [PubMed: 29400714]

Simms CL, Thomas EN, and Zaher HS (2017). Ribosome-based quality control of mRNA and nascent peptides. Wiley Interdiscip. Rev. RNA 8.

Sun Y, Eshov A, Zhou J, Isiktas AU, and Guo JU (2020). C9orf72 arginine-rich dipeptide repeats inhibit UPF1-mediated RNA decay via translational repression. Nat. Commun 11, 3354. [PubMed: 32620797]

Tran H, Almeida S, Moore J, Gendron TF, Chalasani U, Lu Y, Du X, Nickerson JA, Petrucelli L, Weng Z, and Gao FB (2015). Differential Toxicity of Nuclear RNA Foci versus Dipeptide Repeat Proteins in a Drosophila Model of C9ORF72 FTD/ALS. Neuron 87, 1207–1214. [PubMed: 26402604]

Vucic S, and Kiernan MC (2006). Novel threshold tracking techniques suggest that cortical hyperexcitability is an early feature of motor neuron disease. Brain 129, 2436–2446. [PubMed: 16835248]

Vucic S, Nicholson GA, and Kiernan MC (2008). Cortical hyperexcitability may precede the onset of familial amyotrophic lateral sclerosis. Brain 131, 1540–1550. [PubMed: 18469020]

Xu Z, Poidevin M, Li X, Li Y, Shu L, Nelson DL, Li H, Hales CM, Gearing M, Wingo TS, and Jin P (2013). Expanded GGGGCC repeat RNA associated with amyotrophic lateral sclerosis and frontotemporal dementia causes neurodegeneration. Proc. Natl. Acad. Sci. USA 110, 7778–7783. [PubMed: 23553836]

Xu W, Bao P, Jiang X, Wang H, Qin M, Wang R, Wang T, Yang Y, Lorenzini I, Liao L, et al. (2019). Reactivation of nonsense-mediated mRNA decay protects against C9orf72 dipeptide-repeat neurotoxicity. Brain 142, 1349–1364. [PubMed: 30938419]

Yamada SB, Gendron TF, Niccoli T, Genuth NR, Grosely R, Shi Y, Glaria I, Kramer NJ, Nakayama L, Fang S, et al. (2019). RPS25 is required for efficient RAN translation of C9orf72 and other neurodegenerative disease-associated nucleotide repeats. Nat. Neurosci 22, 1383–1388. [PubMed: 31358992]

Zhang K, Donnelly CJ, Haeusler AR, Grima JC, Machamer JB, Steinwald P, Daley EL, Miller SJ, Cunningham KM, Vidensky S, et al. (2015). The C9orf72 repeat expansion disrupts nucleocytoplasmic transport. Nature 525, 56–61. [PubMed: 26308891]

Zu T, Liu Y, Bañez-Coronel M, Reid T, Pletnikova O, Lewis J, Miller TM, Harms MB, Falchook AE, Subramony SH, et al. (2013). RAN proteins and RNA foci from antisense transcripts in C9ORF72 ALS and frontotemporal dementia. Proc. Natl. Acad. Sci. USA 110, E4968–E4977. [PubMed: 24248382]

Highlights

- NMD is unaltered by the *C9orf72* HRE
- UPF1 overexpression reduces *C9orf72* HRE-mediated toxicity *in vitro* and *in vivo*
- UPF1 neuroprotection occurs independently of NMD pathway
- UPF1 neuroprotection may occur through reduction of DPR abundance

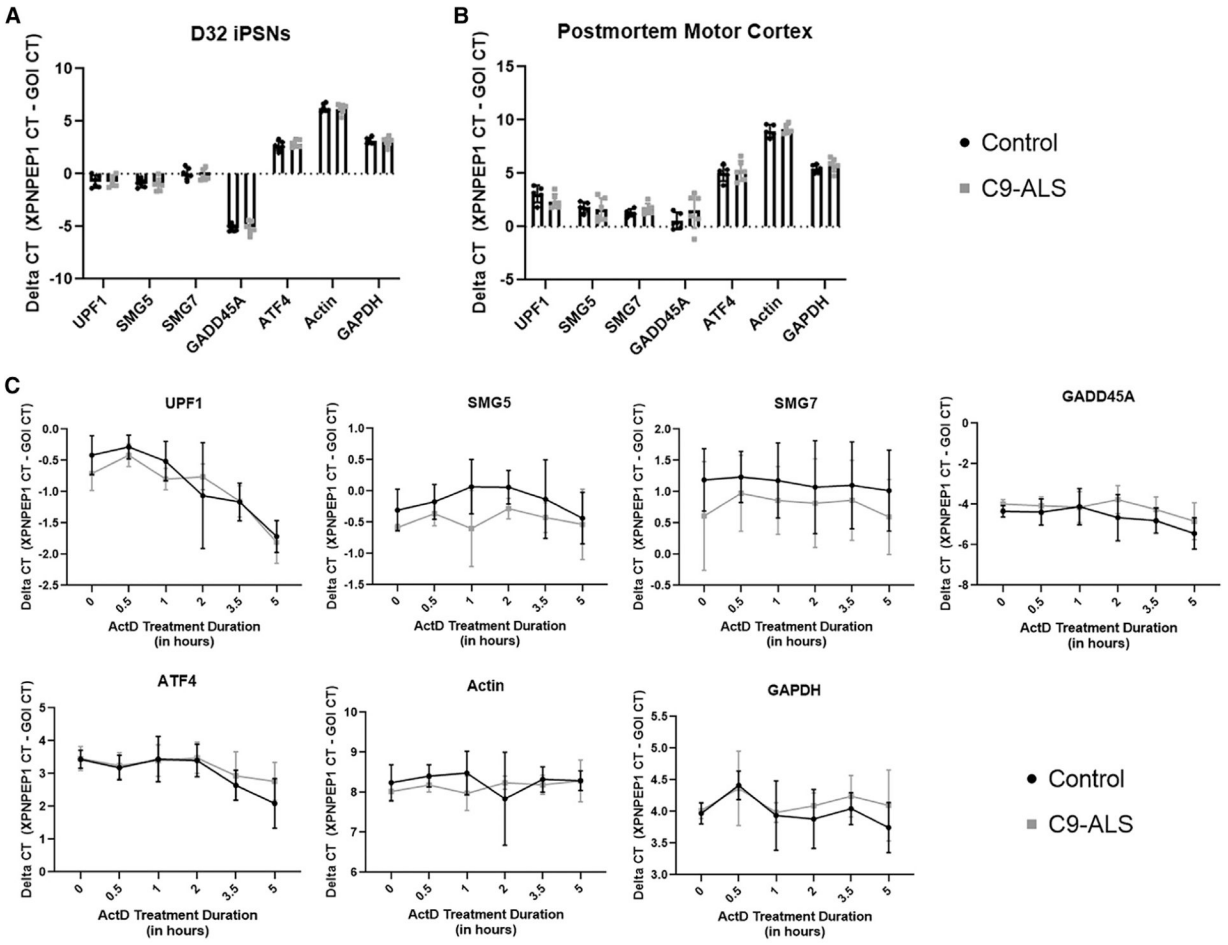

Figure 1. NMD is not altered in C9-ALS iPSNs and postmortem motor cortex of C9-ALS patients

(A) Delta CT of NMD substrates in C9-ALS iPSNs compared to control iPSNs as measured by qRT-PCR (XPNPEP1 mRNA used for normalization). n = 6 pairs of age- and sex-matched control and *C9orf72* iPSNs.

(B) Delta CT of NMD substrates in postmortem motor cortex of C9-ALS patients compared to unaffected individuals as measured by qRT-PCR (XPNPEP1 mRNA used for normalization). n = 5 control and 6 C9-ALS motor cortex samples.

(C) Delta CT of NMD substrates in control and C9-ALS iPSNs following treatment with 10 μg/mL actinomycin D for the time points indicated on the x axis (XPNPEP1 mRNA used for gene normalization, Time 0 used for temporal normalization). n = 4 pairs of age- and sex-matched control and *C9orf72* iPSNs. Two-way ANOVA with Sidak's multiple comparison test was used to calculate statistical significance.

Data are represented as mean ± SD.

See also Figures S1 and S2.

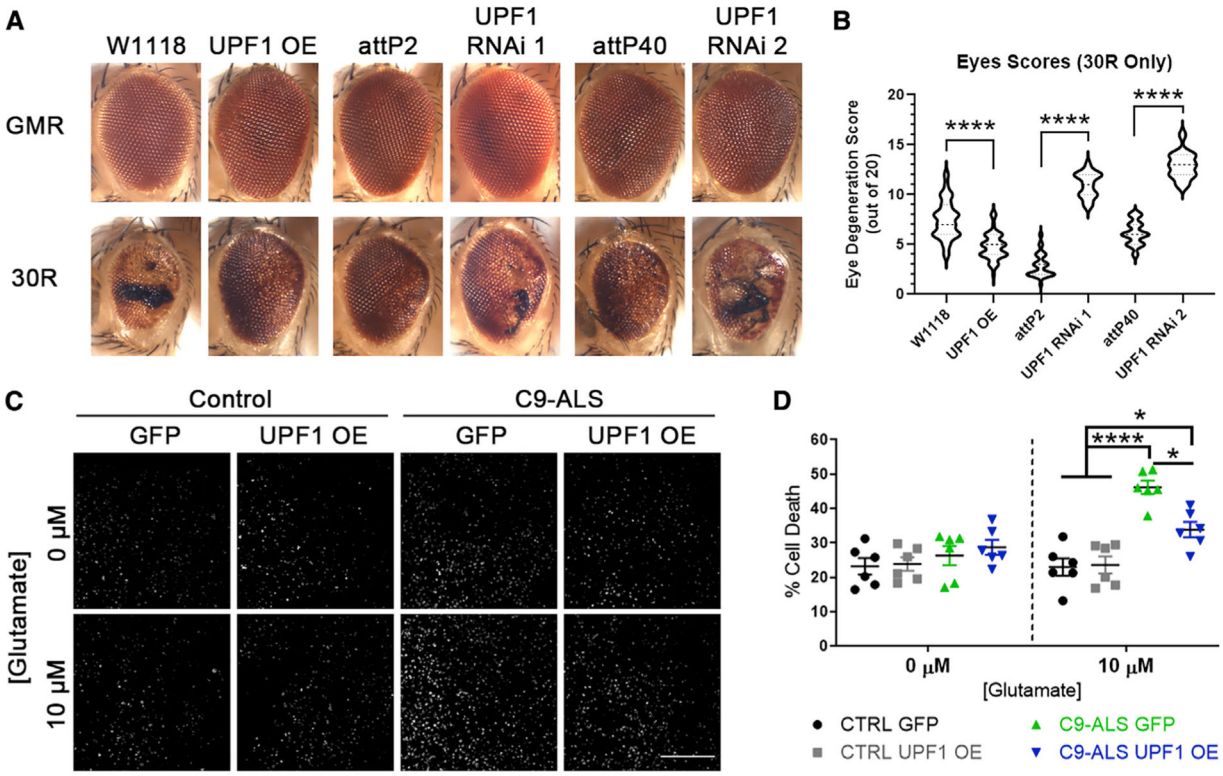

Figure 2. UPF1 OE reduces *C9orf72* HRE-mediated neurodegenerative phenotypes

(A) Representative images of *Drosophila* eyes expressing the noted UPF1 expression modifiers in photoreceptors using a GMR driver. Top images are from flies expressing the noted alleles only, and bottom images are from flies expressing the noted alleles in the context of 30 GGGGCC repeats under the same driver.

(B) Violin plots of eye degeneration scores of 30R flies expressing the noted UPF1 alleles. See Method details for details on scoring method. Two-way ANOVA with Tukey's multiple comparison test was used to calculate statistical significance. ****$p < 0.0001$. From left to right, n = 108, 54, 101, 15, 60, 15. Data are represented as violin plots with indicated quartiles.

(C) Representative fields of view of propidium-iodide-positive iPSNs in the absence (top row) or presence (bottom row) of 10 µM glutamate. Scale bar, 100 µm.

(D) Quantification of the relative proportion of propidium-iodide-positive (dead) cells to total cells from images in (C), represented as "% Cell Death." n = 3 pairs of age- and sex-matched control and *C9orf72* iPSNs, 2 replicates per pair. Six fields of view were analyzed for each data point. Two-way ANOVA with Tukey's multiple comparison test was used to calculate statistical significance. *$p < 0.05$, ****$p < 0.0001$.

Data are indicated as mean ± SD.

See also Figure S3.

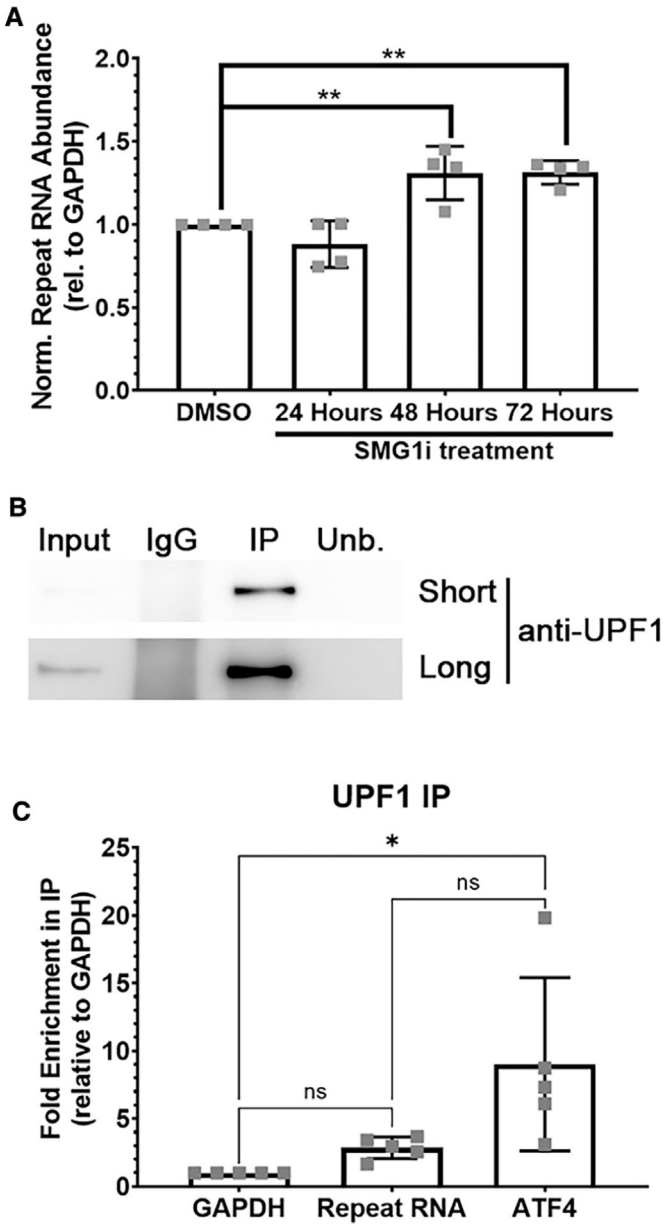

Figure 3. *C9orf72* HRE sense RNA is in a complex with UPF1 and is stabilized by NMD inhibition

(A) Relative abundance of sense repeat RNA following treatment with 0.5 μM SMG1i for the indicated periods of time (24 h 0.1% DMSO treatment used for normalization). n = 4 C9-ALS iPSN lines. Ordinary one-way ANOVA was used to calculate statistical significance. **$p < 0.01$.

(B) Western blot against total UPF1 protein in samples following anti-UPF1 IP from C9-ALS iPSN lysates. Short and long exposures are shown on the top and bottom, respectively.

(C) Fold enrichment of sense repeat RNA and ATF4 mRNA relative to GAPDH in IP fraction following anti-UPF1 pulldown as measured by qRT-PCR (input used for normalization). n = 5 C9-ALS iPSN lines. Ordinary one-way ANOVA was used to calculate statistical significance. *$p < 0.05$.

Data are indicated as mean ± SD.
See also Figure S1.

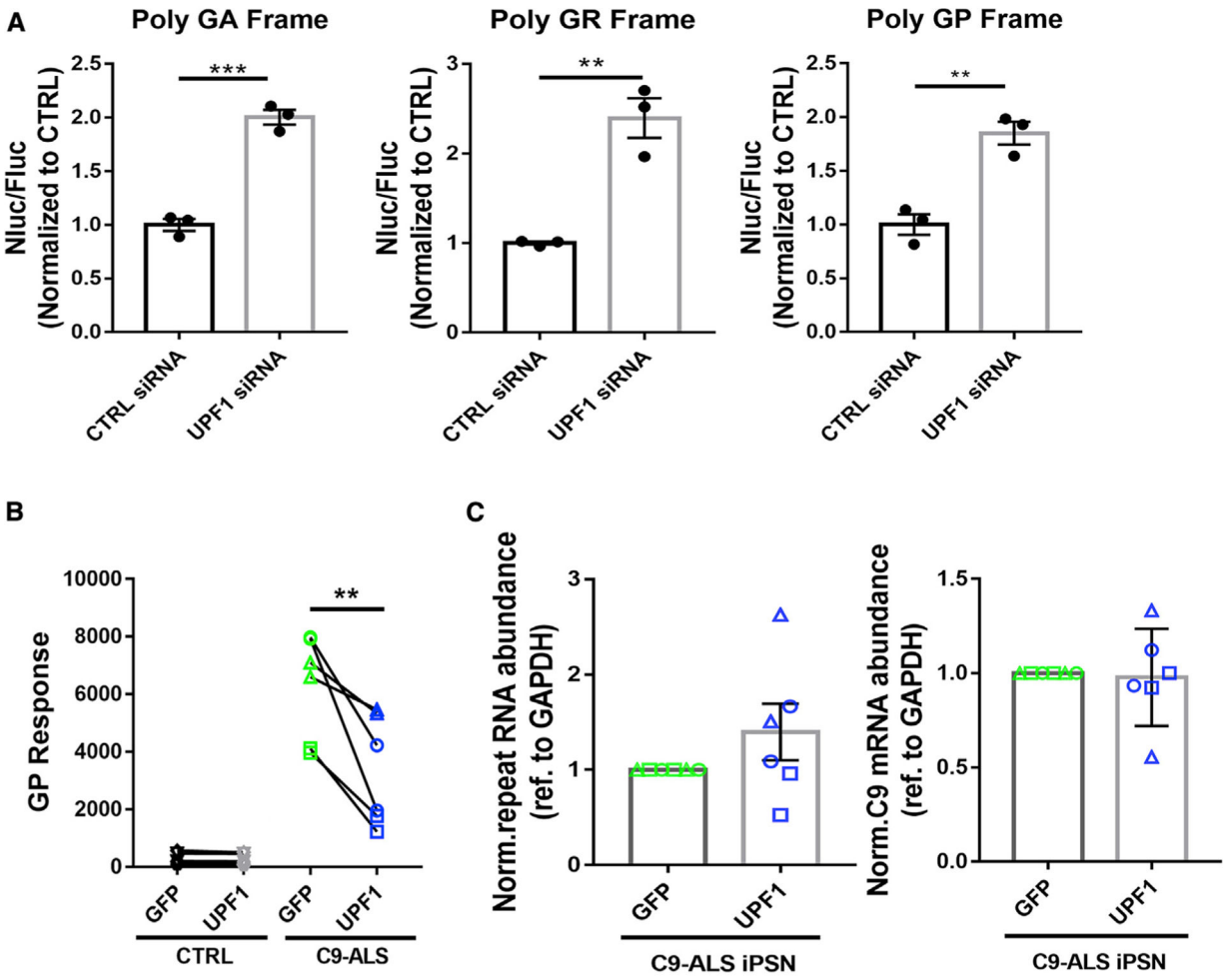

Figure 4. UPF1 expression alters abundance of DPRs

(A) Ratio of Nluc to Fluc from HeLa cells stably expressing dual-luciferase reporters (with reading frame noted) and transfected control or UPF1 siRNA. n = 3 biological replicates. Unpaired t tests were used to calculate statistical significance. **p < 0.01, ***p < 0.001.

(B) Poly(GP) response in control (left) and C9-ALS (right) iPSNs following OE of GFP or UPF1 as measured by an ELISA assay. n = 3 age- and sex-matched pairs of control and *C9orf72* iPSNs, 2 replicates each line. Ordinary one-way ANOVA was used to calculate statistical significance. *p < 0.05.

(C) Relative abundance of sense repeat RNA in C9-ALS iPSNs OE GFP or UPF1. n = 3 C9-ALS iPSN lines, 2 replicates for each line. Paired t tests were used to calculate statistical significance.

Data are indicated as mean ± SD.

See also Figure S4.

KEY RESOURCES TABLE

REAGENT or RESOURCE	SOURCE	IDENTIFIER
Antibodies		
Mouse anti-FLAG	Sigma	Cat#F1804; RRID:AB_262044
Mouse anti-β-actin	Cell Signaling	Cat#3700; RRID:AB_2242334
Rabbit anti-UPF1	ProteinTech	Cat#23379-1-AP; RRID: AB_11232421
Rabbit anti-UPF1	Abcam	Cat#ab109363 RRID:AB_10861979
Rabbit anti-UPF1	Atlas Antibodies	Cat#HPA020857; RRID:AB_1856175
Rabbit anti-phospho-UPF1 (Ser1127)	Millipore	Cat#07-1016 RRID:AB_10805931
Rabbit anti-MAP2	Cell Signaling	Cat#8707; RRID:AB_2722660
Rabbit anti-GP8	Cheng et al., 2019	Rb5278
Chemicals, peptides, and recombinant proteins		
TransIT-LT1	Mirus	Cat#2305
RNAiMAX	Invitrogen	Cat# 13778075
FastStain	G Biosciences	78–634
L-glutamic acid	Sigma Aldrich	Cat#G1251
RNaseOUT	Thermo Fisher Scientific	Cat#10777019
High Capacity cDNA Reverse Transcription Kit	Thermo Fisher Scientific	Cat#4368814
TriZol	Thermo Fisher Scientific	Cat#15-596-018
RIPA Buffer	Sigma-Aldrich	Cat#R0278
SMG1i	CFTR Chemical Compound Program	N/A
Gibson Assembly® Cloning Kit	New England Biolabs	Cat#E5510S
Critical commercial assays		
Actin Taqman Probe	Thermo Fisher Scientific	Hs03023943_g1
ATF4 Taqman Probe	Thermo Fisher Scientific	Hs00909569_g1
GADD45A Taqman Probe	Thermo Fisher Scientific	Hs00169255_m1
UPF1 Taqman Probe	Thermo Fisher Scientific	Hs00161289_m1
GGGGCC Repeat RNA Taqman Probe	Lagier-Tourenne et al., 2013	N/A
C9ORF72 Taqman Probe	Lagier-Tourenne et al., 2013	N/A
SMG5 Taqman Probe	Thermo Fisher Scientific	Hs00392882_m1
SMG7 Taqman Probe	Thermo Fisher Scientific	Hs00208049_m1
XPNPEP1 Taqman Probe	Thermo Fisher Scientific	Hs00958021_m1

REAGENT or RESOURCE	SOURCE	IDENTIFIER
Nano-Glo Dual Luciferase Assay	Promega	Cat#N1620
Experimental models: Cell lines		
Human: HeLa Flp-In dual luciferase reporter cells	Cheng et al., 2019	N/A
Human: iPS cell CS7VCZiALS	Cedars-Sinai Induced Pluripotent Stem Cell (iPSC) Core	https://www.cedars-sinai.edu/Research/Research-Cores/Induced-Pluripotent-Stem-Cell-Core-/
Human: iPS cell CS0NKCiALS	Cedars-Sinai Induced Pluripotent Stem Cell (iPSC) Core	https://www.cedars-sinai.edu/Research/Research-Cores/Induced-Pluripotent-Stem-Cell-Core-/
Human: iPS cell EDi036-A	Cedars-Sinai Induced Pluripotent Stem Cell (iPSC) Core	https://www.cedars-sinai.edu/Research/Research-Cores/Induced-Pluripotent-Stem-Cell-Core-/
Human: iPS cell CS8PAAiCTR	Cedars-Sinai Induced Pluripotent Stem Cell (iPSC) Core	https://www.cedars-sinai.edu/Research/Research-Cores/Induced-Pluripotent-Stem-Cell-Core-/
Human: iPS cell EDiO37-A	Cedars-Sinai Induced Pluripotent Stem Cell (iPSC) Core	https://www.cedars-sinai.edu/Research/Research-Cores/lnduced-Pluripotent-Stem-Cell-Core-/
Human: iPS cell CSOBUUiALS	Cedars-Sinai Induced Pluripotent Stem Cell (iPSC) Core	https://www.cedars-sinai.edu/Research/Research-Cores/lnduced-Pluripotent-Stem-Cell-Core-/
Human: iPS cell CS6UC9iALS	Cedars-Sinai Induced Pluripotent Stem Cell (iPSC) Core	https://www.cedars-sinai.edu/Research/Research-Cores/lnduced-Pluripotent-Stem-Cell-Core-/
Human: iPS cell EDiO43-A	Cedars-Sinai Induced Pluripotent Stem Cell (iPSC) Core	https://www.cedars-sinai.edu/Research/Research-Cores/lnduced-Pluripotent-Stem-Cell-Core-/
Human: iPS cell EDiO29-A	Cedars-Sinai Induced Pluripotent Stem Cell (iPSC) Core	https://www.cedars-sinai.edu/Research/Research-Cores/lnduced-Pluripotent-Stem-Cell-Core-/
Human: iPS cell CS6CLWiALS	Cedars-Sinai Induced Pluripotent Stem Cell (iPSC) Core	https://www.cedars-sinai.edu/Research/Research-Cores/lnduced-Pluripotent-Stem-Cell-Core-/
Human: iPS cell EDiO34-A	Cedars-Sinai Induced Pluripotent Stem Cell (iPSC) Core	https://www.cedars-sinai.edu/Research/Research-Cores/lnduced-Pluripotent-Stem-Cell-Core-/
Human: iPS cell CS6ZLDiALS	Cedars-Sinai Induced Pluripotent Stem Cell (iPSC) Core	https://www.cedars-sinai.edu/Research/Research-Cores/lnduced-Pluripotent-Stem-Cell-Core-/
Human: iPS cell CS9XH7iCTR	Cedars-Sinai Induced Pluripotent Stem Cell (iPSC) Core	https://www.cedars-sinai.edu/Research/Research-Cores/lnduced-Pluripotent-Stem-Cell-Core-/
Human: iPS cell CS0002iCTR	Cedars-Sinai Induced Pluripotent Stem Cell (iPSC) Core	https://www.cedars-sinai.edu/Research/Research-Cores/lnduced-Pluripotent-Stem-Cell-Core-/

REAGENT or RESOURCE	SOURCE	IDENTIFIER
Experimental models: Organisms		
D. melanogaster: GMR-Gal4. w[1118]; P{w[+mW.hs] = GawB}VGlut[OK371]	BDSC	BDSC: 1104
D. melanogaster. 30R: w[1118];UAS-$(G_4C_2)_{30}$	Xu et al., 2013)	FlyBase: FBal0294759
D. melanogaster. UPF1 OE: w[*]; P{w[+mC] = UASp-GFP.Upf1}2	BDSC	BDSC: 24623
D. melanogaster. UPF1 RNAi 1: y[1] v[1]; P{y[+t7.7] v[+t1.8] = TRiP.GL01485}attP2	BDSC	BDSC: 43144
D. melanogaster. UPF1 RNAi 2: y[1] sc[*] v[1] sev[21]; P{y[+t7.7] v[+t1.8] = TRiP.HMC05537}attP40	BDSC	BDSC: 64519
D. melanogaster. TRiP background control, attP2: y[1] v[1]; P{y[+t7.7] = CaryP}attP2	BDSC	BDSC: 36303
D. melanogaster. TRiP background control, attP40: y[1] v[1]; P{y[+t7.7] = CaryP}attP40	BDSC	BDSC: 36304
D. melanogaster. W1118 background control: W[1118]		FlyBase: FBal0018186
Oligonucleotides		
UPF1 Forward	This manuscript	gggaaTCTAGAACCATGAGCGTGGAGGCGTACGG
UPF1 Reverse	This manuscript	gggaaGGATCCtttatcgtcatcgtctttgtagtcATACTGGGACAGCCCCGTCA
R843C Fragment 1 Forward	This manuscript	CTTTCAGGGATGCGAGAAGGACTTCATCATCCTGTCCTGT
R843C Fragment 1 Reverse	This manuscript	TCAGAATGACTTGGTTGAGTACTCACCAGTCACAGAAAAG
R843C Fragment 2 Forward	This manuscript	CTTTTCTGTGACTGGTGAGTACTCAACCAAGTCATTCTGA
R843C Fragment 2 Reverse	This manuscript	GTCCTTCTCGCATCCCTGAAAGGCGTCCACACTGGCGATC
R843C Sequencing	This manuscript	CCTGGTGCAGTACATGCAG
Non-Targeting siRNA	GE Dharmacon	Cat#D-001810-10-05
Pooled UPF1 siRNA	GE Dharmacon	Cat# L-011763-00-0005
Recombinant DNA		
Plasmid: Lenti-UPF1-FLAG	This manuscript	N/A
Plasmid: Lenti-UPF1 (R843C)-FLAG	This manuscript	N/A
Plasmid: Lenti-GFP	Cheng et al., 2019	N/A
Software and algorithms		
FIJI	NIH	https://imagej.net/Fiji
Graph Pad Prism 7	Graph Pad	https://www.graphpad.com/scientific-software/prism/
Graph Pad Prism 8	GraphPad	https://www.graphpad.com/scientific-software/prism/
ImageJ	NIH	https://imagej.nih.gov/ij/
Illustrator	Adobe	RRID:SCR_010279
Other		
Zeiss Apotome	Carl Zeiss	N/A
Micro Confocal High-Content Imaging System	Molecular Devices	N/A

REAGENT or RESOURCE	SOURCE	IDENTIFIER
Applied Biosystems Step One Plus Real Time PCR Machine	Thermo Fisher Scientific	Cat#4376600
QuantStudio 3 Real-Time PCR System	Thermo Fisher Scientific	N/A
ImageQuant LAS 4000	GE Healthcare	N/A